Secure On-skin Biometric Signal Transmission using Galvanic Coupling

William J. Tomlinson*, Stella Banou*, Christopher Yu**, Michele Nogueira***, and Kaushik R. Chowdhury*

* Northeastern University,Boston MA, USA, Email: {wjtomlin, sbanou, krc}@ece.neu.edu
**Draper Laboratory, Cambridge MA, USA, Email: cyu@draper.com
***Federal University of Parana, Curitiba, PR, Brazil, Email: michele.nogueira@ufpr.br

***Abstract*—Increasing threats of malicious eavesdropping raise concerns in confidential data reporting by body-worn sensors. We propose a secure, body-guided transmission channel through the use of galvanic coupling (GC). This method involves injecting weak electrical current into the body, which propagates primarily through the skin. The proposed approach makes the transmission of biometric data impervious to sniffing attacks, enabling the body to serve as a waveguide. This paper makes the following contributions: (i) An analytical channel model using a tissue equivalent circuit of the human arm-wrist-palm GC-propagation path is formulated and empirically verified. (ii) A simulation study is conducted for a comparative analysis of various modulation schemes, leveraging the validated GC-channel behavior. (iii) A GC-transceiver with optimized communication parameters (modulation, frequency, power) is designed and implemented using a dielectrically equivalent tissue phantom, and (iv) through experimental trials, resilience to over-the-air susceptibility (i.e., likelihood of adversarial eavesdropping) of the GC-signal and similar body communication techniques are demonstrated. Performance results of the GC-transceiver prototype yield a bit error rate of 10^{-6} with a transmit power of -2 dBm, in addition to over 7x reduction of signal radiation outside the body compared to capacitive coupling.**

I. Introduction

With the expansion of the wearable technology ecosphere, the pervasiveness of the Internet of Things (IoT), and more recently, the *tactile* IoT, are enabling the human-in-the-loop in unprecedented ways. From body worn sensors to actively controlling smartphones via touch inputs, we continuously communicate large amounts of personal data with the outside world. The prevalent secure communication methods rely on antiquated biometrics or the transmission of secure keys through wireless channels. However, as we argue next, these forms of inputs can be easily spoofed and are highly susceptible to intentional eavesdropping and privacy-manipulation enabled by off-the-shelf but sophisticated software defined radios. Instead of using an over-the-air channel and traditional biometrics, we propose a radically different communication pathway to transmit biological signals containing advanced biometric information collected (via on-body sensors) in real-time. Our approach uses on-skin conduction through a technique called galvanic coupling (GC), where weak electrical currents are modulated with information and then injected into the human tissue [1].

•**Limitations of existing biometrics and passwords:** Despite the ubiquitous use of biometrics like fingerprints, retina/iris and facial features for commercial use, mobile devices still utilize auxiliary passwords for additional forms of secure communication. The use of traditional passwords often yields drawbacks in terms of user recollection, password strength and scale.

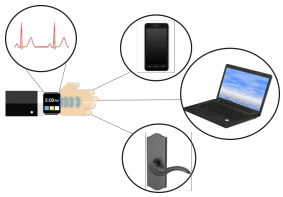

Fig. 1: A biological signal is acquired by a wrist-worn device and transmitted through the human skin to unlock devices by physical contact.

Fingerprints, although unique, are transferable and can be left on various surfaces that users have daily interaction with. Such vulnerabilities are exploited via plastic, latex or gelatin based molds, used to forge a copy of the individuals biometric. Additionally, high resolution images/videos are used in counterfeiting retina and facial recognition software [2], [3]. Hence, we believe that a new class of biophysical signals drawn from within the user's own body, such as the well-known electrocardiogram (ECG) signal [3], can yield high levels of individual distinction [4] and has found increasing use in secure communication [5]. Capturing and relaying these signals to an external point remains an open challenge, which we propose to tackle in this paper.

•**Limitations of over-the-air RF:** Although research on key generation and sharing for wireless sensors has made rapid strides, increasingly sophisticated sniffing attacks, coupled with limited computational resources within the sensors, pose practical limitations. Instead, we propose an alternate method of transmitting information securely using GC that bypasses the vulnerable RF transmission channel. GC uses weak electrical current (0.5mA) that is modulated by the information to be transmitted. This data carrying signal is coupled to the body tissue, here the skin surface, by simple, small form-factor electrodes. By setting the frequency in the range 100kHz-1MHz, the signal energy is largely retained within the human tissue [1]. Thus, with negligible amount of external radiation, it mitigates sniffing attacks. The only way to intercept the signal is to physically touch the subject with a pair of receiving

electrodes.

•Proposed Approach: Secure biometric transmission with GC: Our proposed system, envisioned in Figure 1, is composed of a wearable (here, we show a specific use-case for the upper forearm band that allows transmission of ECG signals, though any other signal/body location can be chosen), as opposed to intrusively implanting devices. The device non-invasively acquires a biological signal, extracts unique features and modulates a weak electric current to create the non-radiating GC-waveform. This GC-signal is transmitted wirelessly through the arm, wrist and palm of the subject to the receiver, be it a data logging entity, actuation interface (e.g., door handle) or a smart-device. The receiver has a GC front-end that captures the signal and then feeds it to a classifier for pattern matching.

The main contributions of our work are as follows:

1) We design and experimentally validate an electrically-equivalent circuit model of the human arm-wrist-palm tissue channel and characterize the behavior of the GC-signal. We use the results of our channel studies to optimize the design of transmission parameters and modulation schemes for the galvanic coupling communication system.
2) Through experimental evaluation, we show how the GC-signal emits minuscule levels of signal radiation outside the body compared to the well-studied Capacitive Coupling (CC) and similar solutions for body-guided communication. Furthermore, we show that our use of the GC-signal makes it virtually unfeasible to decode data over-the-air at an adversarial receiver.
3) We implement a proof-of-concept secure biometric transmission system using the Teensy™ microcontoller unit that supports analog front-end hardware for transmission and reception of GC-signals.
4) We demonstrate the link performance of our prototype by transmitting sample ECG data (provided by PhysioNet [6]) with a bit-error-rate (BER) of 10^{-6} and a transmit power of -2 dBm. Moreover, all data files and software code are available to the community for repeatability of experiments.

II. RELATED WORK

A. Galvanic vs Capacitive Coupling

A plethora of intra-body communication (IBC) techniques have been widely studied in the literature (e.g., ultrasound, magnetic resonance coupling) [7]. In this work, we study methods that have been more commonly applied towards biometric authentication solutions. Specifically, we focus on coupling-based IBC methods that are classified into two types based on the nature of propagation. The first method, which we utilize in this work, is known as Galvanic Coupling (waveguide based). The second, Capacitive Coupling (electric-field based), also employs a pair of electrodes at the transmitter and receiver terminals [8]. In the GC method, both transmitter and receiver electrodes are attached to the body (with individual references) and alternating current is injected differently between the transmitter electrodes. A dominant source of current will flow between the positive and negative terminals of the transmitter, but a weaker, secondary current will flow throughout the tissues where the receiver electrodes will measure the potential difference across them [9]. In the Capacitive Coupling (CC) method, the signal electrode of the transmitter and the receiver are typically attached (or placed in close proximity) to the human body while the ground electrodes are floating, thereby capacitively coupling the human body to its surrounding environment. The signal electrode of the transmitter induces an electric field into the human body. The induced electrical signal is controlled by an electrical potential and the body acts as a floating conductor with the ground as the return path [10]. Unfortunately, this behavior makes capacitive coupling more susceptible to motion and external interference (e.g., power line, objects with conducting surfaces and potentially neighboring capacitively coupled body networks) [11]. Galvanic coupling signals, although more sensitive to body locations, body composition, electrode orientation and inter-electrode distances, are confined within the human tissue layers and thus are virtually unaffected by outside environmental conditions [9]. We exploit this feature to enable secure side-channel communication for the transmission of biometric data.

B. Galvanic Coupling Equivalent Circuit Channel Modeling

Extensive work has been done in [1], [12] to analytically model the human body channel as a complex network of impedances, representing the different layers of human tissue and their boundaries. For example, in [1], each layer of human tissue is modeled as combination of electrical circuits that constitute a 2-port network for the computation of signal gain at an output terminal. The implementation of the 2-port circuit model allows easy modification of parameters (center frequency, electrode separation, electrode dimensions, etc.) and flexibility in terms of transmitter and receiver placement. Previous methods of channel modeling, although highly complex and well inclusive of the dielectric properties of human tissue, assume uniformity across all signal paths and tissue layers, such as an end-to-end propagation cross-section as a single, homogeneous medium. Therefore, the channel modeling conducted in this work focuses on a 3D tissue equivalent circuit model with varying dimensions that adequately reflect the portion of the body used as a communication medium.

C. Galvanic Coupling Communication Systems

Experimental platforms and testbeds using GC have been proposed in [13], [9]. In [13] differential binary phase-shift-keying (DBPSK) modulation is selected given its robustness to amplitude variations and minimal hardware complexity when compared to coherent schemes. The work conducted in [9] proposes a pulse position modulation ultra wideband system and follows the specifications of the physical layer outlined in IEEE 802.15.6 for Wireless Body Area Networks. However, these systems offer macro-scale representations of the transmitter and/or receiver architecture, characteristics not

yet applicable for the wearable device arena. Additionally, there is no example application with packet-level framing of data demonstrated earlier, as the main focus is to conduct empirical analysis to verify channel behavior. In contrast, our work focuses on the sending and receiving of biological data via GC, with a system design focused on operation in the wearable domain.

D. Body-Guided Authentication Systems

In the commercial space, the Nymi Band [5] is a wearable authenticator designed to work with other devices (desktop computers, doors, etc.) and perform authentication based on proximity to the locked device. The Nymi band employs a biological signal (e.g., Lead I ECG measurements) as a biometric. Once a user is authenticated, it uses Bluetooth Low Energy and NFC to pair with devices running the Nymi supported application. The works presented in [14] and [15] enable continuous authentication with commodity devices using capacitive coupling body communication. Specifically, [14] proposes an impedance measurement biometric system with a touch sensing mechanism. This data is modulated through the user's body using an On-Off Keying approach. Additional CC-based examples of touch based authentication systems are listed in [10], where a wrist-worn tag, containing a unique ID key, exchanges information with a receiver through touch. Similarly, the work in [16] presents a touch enabled body communication system for multimedia-based applications by encoding information on captured electromagnetic interference data. The above-mentioned studies show great potential for using biological data as a biometric and the utility of proximity/touch-based communication and authentication. However, all the above wireless communication methods using classical RF or CC still operate over-the-air, and thus are susceptible to eavesdropping, data interception, or data/fault injection (as we show later in Section VI). Thus, we are motivated to develop a secure GC-based surface-to-surface communication by avoiding the over-the-air medium.

III. GC Channel Model for Arm-Wrist-Palm

Our approach relies on a carefully tuned physical layer optimized with respect to the arm-wrist-palm path that is employed to relay biometric information. This is a generic pathway, which can be adapted for other tissue segments. We depart from the assumption of tissues resembling homogeneous cylinders in [1], but we retain the concept of creating an electrical equivalent circuit. Key assumptions that we make in this work (also validated later through experiments) are: (i) the section of the arm where the biometric signal is retrieved, and then forwarded through the wrist area, is cuboidal in shape; and (ii) the thickness and properties of each tissue layer, i.e., skin, fat, tendon, muscle, bone are uniform within the separate partitioned segments that form the arm, wrist and palm.

We separately analyze the propagation from the three parts of the path: the arm, wrist and palm. We first begin by identifying typical tissue thickness and propagation characteristics of each of these three segments. For example, a segment consists

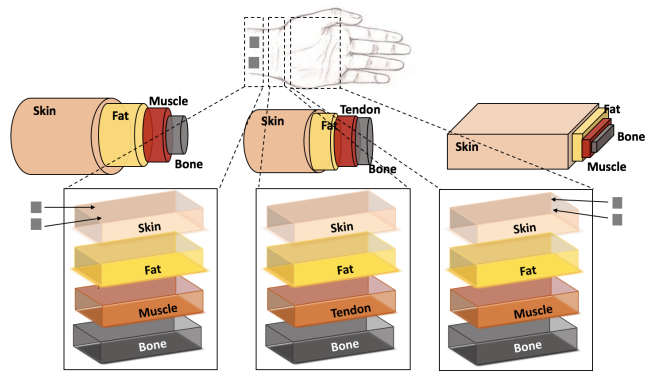

Fig. 2: Cubical approximation of arm, wrist and palm parts, and location of electrode attachment for galvanic coupling

of four layers: skin, fat, muscle and bone for the arm and skin, fat, tendon and bone for the wrist (Figure 2). Through cubical approximation for the arm and wrist segments, the final representation of the path is simplified to three rectangular shapes with four tissue layers of specific thicknesses. The next step is to analyze the path to estimate its channel gain based on the dielectric properties and dimensions of the tissue layers.

A. Tissue Equivalent Circuit

GC requires two transmitting and two receiving electrodes attached on the skin. Thus, we formulate a tissue equivalent circuit (TEC) model to estimate the channel gain of the path between the arm and the palm. The impedance between two nodes of the TEC is calculated using an RC-circuit equivalent expression of the given path. The resistance and capacitance values of each path are calculated as $R = \frac{\rho L}{A_c}$ and $C = \frac{\epsilon A}{D}$.

The resistivity (ρ) and permittivity (ϵ) values for each tissue layer are frequency dependent and obtained from a published, standardized database [17]. Here, L represents the length of the path between the two nodes, A_c gives the cross-sectional area of the path, A is the surface area of the capacitance measured and D is the depth of the tissue. After calculating the resistance and capacitance of the path between two nodes, the impedance of the specific path is calculated using $Z = R + \frac{1}{C\omega i}$.

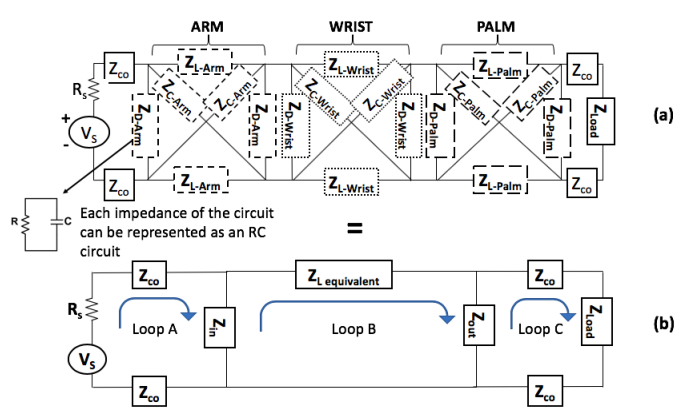

Fig. 3: Circuit (a) is the TEC of the skin layer in 2D. (b) is the equivalent of (a) used for channel gain calculations

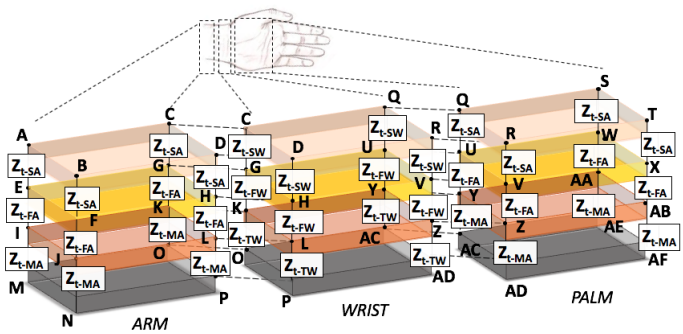

Fig. 4: 3D tissue equivalent circuit with transverse impedances for arm-wrist-palm path. The labeling of transverse impedances is Z_{t-ij}, for i ∈ [S, F, M, T, B] corresponding to skin, fat, muscle, tendon, bone and j ∈ [A, W, P] for arm, wrist, palm

The impedance, resistivity, permittivity, length, cross-sectional area, surface area and thickness values are inputs to the model that we formulate next. The TEC for the entire path requires the calculation of five impedance values: Z_L (longitudinal), Z_D (inter-electrode), Z_C (cross) and Z_t (transverse), trivially obtained by replacing the respective ρ, ϵ, L and A values depending on the geometry of the path and using the above standard equations. The topview of the TEC is shown in Figure 3. The transverse impedance Z_t is between each layer and its adjacent one. A 3D representation of the TEC including the Z_t is depicted in Figure 4. The nodes are shown via capitalized letters; the arm-wrist and wrist-palm junctions share nodes. Hence, the Z_D and Z_t values are calculated by adding the two inverse impedances of the specific paths, as these impedances are parallel to each other, as also seen in the top-view of Figure 3.

We perform a nodal analysis using Kirchoff's Current Law (KCL) with the impedance of all paths to obtain an admittance matrix for the entire four-layer, thirty-two node equivalent circuit. For a sample node A, the nodal equation is:

$$I = \frac{V_A - V_B}{Z_D} + \frac{V_A - V_C}{Z_L} + \frac{V_A - V_D}{Z_C} + \frac{V_A - V_E}{Z_t} \tag{1}$$

Similarly, the equations for all nodes were derived, but not repeated here for space conservation. A simplified representation of the 32 KCL equations is the admittance matrix (A) of the 4-layer 3D circuit in equation (1).

To obtain the gain of the TEC if a voltage is applied at the input terminals, an equivalent Pi-network is derived (Figure 4 (b)). The purpose of this step is to analyze the TEC as a two-port network with Z-parameters for the gain calculation. The Z-parameters of the circuit in Figure 4 (b) are calculated with Equations (3) - (6) which were derived from a 3-loop mesh analysis (loops A, B and C in Figure 3(b)), adhering to the two-port network parameter definitions.

$$z_{11} = R_s + 2Z_{co} + \frac{Z_{in}(Z_{Leq} + Z_{out})}{Z_{Leq} + Z_{in} + Z_{out}} \tag{3}$$

$$z_{21} = \frac{Z_{in}Z_{out}}{Z_{Leq} + Z_{in} + Z_{out}} \tag{4}$$

$$z_{12} = -\frac{Z_{in}Z_{out}}{Z_{Leq} + Z_{in} + Z_{out}} \tag{5}$$

$$z_{22} = 2Z_{co} + \frac{Z_{out}(Z_{Leq} + Z_{in})}{Z_{Leq} + Z_{in} + Z_{out}} \tag{6}$$

For example, Equation (3) calculates the z_{11} parameter (expressed as a ratio of the input voltage over the input current), by setting the current in Loop C equal to zero. The expressions for input voltage and current are subsequently derived from the resulting 2-loop circuit (loops A and B).

In summary, our model takes as input the length of the arm, wrist and palm, the size and distance between transmitting and receiving electrodes as well as the signal frequency. The admittance matrix is then constructed using the equations and inputs of the model. The gain of the entire arm-wrist-palm path is then calculated as the logarithmic ratio of the impedance over the output (between nodes S and T) and that of the input (between nodes A and B). The gain of the channel can be investigated using the model under several configurations and plays an important role in the design parameters of the GC communication system. The 3D arm-wrist-palm model is validated experimentally, in the next subsection, for various scenarios. Subsequently, we utilize the knowledge of the channel response to test and compare various aspects of the GC communication system design in MATLAB, before we demonstrate the implementation of a real system.

B. Experimental Model Validation

The proposed model is used to obtain (i) distances at which the gain of the channel is high (as we shall show later, the gain shows non-uniform behavior), and (ii) to set the frequency of operation and inter-electrode distance. For these reasons, we first validate the arm-wrist-palm model through an experimental setup. We conduct experiments on an electrically equivalent synthetic tissue phantom from Syndaver Labs™ that represents the human arm, wrist and palm components. For all reported experimental results, the gain between different parts of the phantom is calculated by measuring the input and output Peak-to-Peak voltage of a sinusoid at various distances. The Analog Discovery ™ module is used as both a waveform generator and oscilloscope to transmit a sinusoid and read the signal at different parts of the phantom, respectively. To avoid the use of a common ground between input and output, two Analog Discovery devices are employed, each with its own PC connection. Balun circuits (Schaffner IT239) bridge the connection between the phantom and the Analog Discoveries. This aids in additional isolation of the common ground return path that can be caused by the lack of EMI shielding and large base of the laptops (transmitter and receiver) attached to the same surface. The skin-to-skin channel gain is important as it is the main propagation path of the smart-device. Therefore, the wires of the oscilloscope measuring voltage as well as the function generator are attached to the skin of the phantom. We model the edge of the wires that are attached on the skin

$$A = \begin{bmatrix} \sum_{i \in C,L,D,t} \frac{1}{Z_{iSA}} & -\frac{1}{Z_{Dsa}} & -\frac{1}{Z_{Lsa}} & \cdots & \cdots & \cdots & \cdots & 0 \\ -\frac{1}{Z_{Dsa}} & \sum_{i \in C,L,D,t} \frac{1}{Z_{iSA}} & -\frac{1}{Z_{Csa}} & -\frac{1}{Z_{Lsa}} & 0 & -\frac{1}{Z_{tsa}} & \cdots & 0 \\ \ddots & \ddots & \ddots & \ddots & \ddots & \ddots & \ddots & \ddots \\ 0 & \cdots & \cdots & \cdots & -\frac{1}{Z_{Tmp}} & -\frac{1}{Z_{Cbp}} & -\frac{1}{Z_{Lbp}} & -\frac{1}{Z_{Dbp}} \end{bmatrix} \quad (2)$$

as electrodes with <1 mm surface area to accurately represent the experimental configuration.

Figure 5a depicts the results of the model validation. Both the experimental setup and our model maximize the gain between 200 and 500 KHz. The gains over a 10 cm distance are overall higher than those for 15 cm, as expected, and match the trends associated with the model predictions for all frequencies. The varying hydration levels of skin layer measurements, shown in [1], support the claim that a deviation between model and experimental data of 5 dB or less provides suitable results. Henceforth, we specifically focus on the gain prediction at around 10 cm distance, which is most relevant to our biometric-based secure communication.

Noting the frequency range where the gain is the highest, we conducted a series of experiments with varying distances between the palm and the arm, to test the reliability of the model as the input parameter of distance changes. This captures possible relative positions of the wristband and the mobile device. Figure 5b shows the gain of a sinusoidal input operating at 400 kHz over various distances by altering the palm and arm lengths. We draw two conclusions from the results: the model closely predicts the gain with varying distances, though varying the length of the palm portion of the path leads to increasing variation in gain than the arm portion. A possible explanation of this phenomenon is the increased thickness of the palm skin layer. Since the gain is calculated on the skin layer, the thickness of the skin affects the gain to a significant extent. When we vary the arm and palm distances around the wrist, we see that the predicted versus observed gain values lie within an acceptable experimental margin of error (Figure 5c). As expected, the gain is highest for shorter distances between transmitter and receiver.

Finally, we study the impact of the inter-electrode separation for the two GC transmitting and receiving electrodes. Results indicate that greater inter-electrode distance between the individual pairs of the transmitting and receiving electrodes leads to a higher gain between the transmitter-receiver nodes, when all other parameters remain constant. Greater inter-electrode distance in galvanic coupling leads to a higher potential between the two electrodes, and therefore, a higher gain between transmitter and receiver. Similar to the previous experiments, the model predictions match closely with the experimental results, proving once again that the arm-wrist-palm model can predict the channel behavior with high accuracy (Figure 5d).

With the theoretical model validated, we focus next on the communication system and its prototype design.

.

TABLE I: Tissue thickness values (mm)

	Skin	Fat	Muscle	Tendon	Bone
Arm	1.00	7.00	15.00	-	20.00
Wrist	1.00	7.00	-	1.50	15.30
Palm	1.40	7.00	9.00 [18]	-	9.17 [19]

IV. Choice of GC modulation scheme

The GC channel model, proposed in Section III-A and experimentally validated in Section III-B, is the starting point of our communication system design. We employ the use of the analytical channel model to store the channel frequency response for reproducible simulations. We then create multiple realizations of the channel behavior by flexibly controlling the center frequency, inter-electrode separation and the amount of arm and palm channel lengths to find the transmitter and receiver link configurations that yield the highest gain values. We select the best combinatorial approach from these parameters and formulate a channel frequency response to test multiple candidate narrow-band modulation schemes and various transmission bandwidths (those that yield flat fading characteristics) using MATLAB. Since we have a tighter constraint on power consumption as opposed to available bandwidth, non-coherent systems and/or techniques with lower modulation orders are more suited for our application. Our goal is to achieve a target BER of 10^{-4} or better by selecting one of: Binary Frequency Shift Keying (BFSK), On-Off Keying (OOK) and Binary Phase Shift Keying (BPSK).

A. Power Consumption Analysis

In order to investigate the power consumption of each system, we model the power required for all analog front-end components depicted in the aforementioned modulation schemes in the MATLAB environment. This model is based on [20], where signal bandwidth, peak-to-average-power ratio (PAPR), modulation order, and channel gain at various frequencies have an affect on the performance. The overall energy consumption of a system, which depends on its front-end components, is calculated in [20] with Equation (7).

$$E_c = ((P_{Tx} + P_{out}) \cdot T_{on}) + (P_{Rx} \cdot R_{on}) \quad (7)$$

The variables P_{Tx} and P_{Rx} represent the total power consumption from the transmitter and receiver electronics, respectively. These values are obtained from the sum of the contribution from the individual components of each system design, which consist of a variation of one or more of analog front-end devices modeled above. The output power (P_{out})

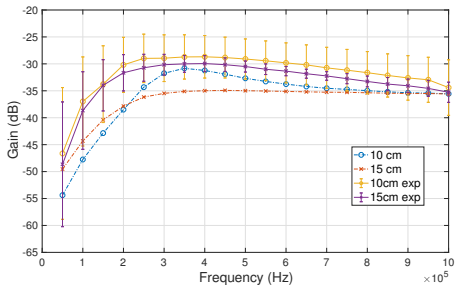

(a) Experimental and model data comparison for gain vs. frequency

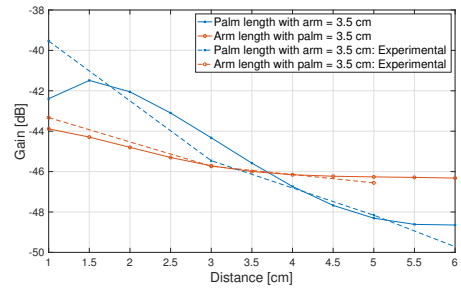

(b) Experimental and model data comparison for gain vs. distance, varying palm length (f_c = 400 kHz)

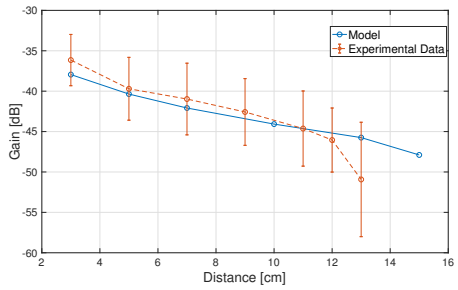

(c) Experimental and model data comparison for gain vs. distance (f_c = 400 kHz)

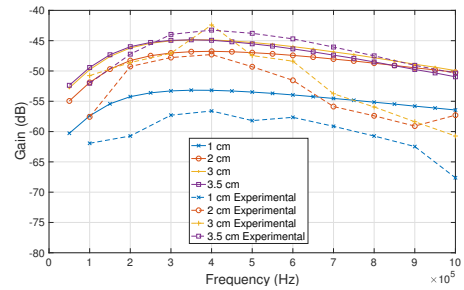

(d) Experimental and model data comparison of gain vs. frequency for varying electrode separation distances

Fig. 5: 3D tissue equivalent model validation

TABLE II: GC-IBC PHY layer performance comparison

System	Occupied Bandwidth	Min. Tx Power	Max Bit rate	Energy Consumption	Modulation Order
BFSK	209.5 kHz	-8 dBm	50 kbps	590.5 μJ	2
BPSK	52.3 kHz	-13 dBm	50 kbps	2.75 mJ	2
OOK	52.57 kHz	-9 dBm	50 kbps	158.2 μJ	2

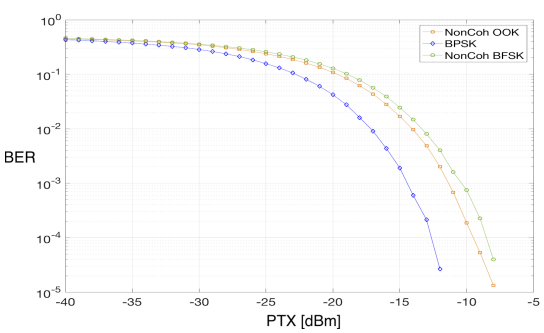

Fig. 6: BER vs transmit power for various modulation schemes

required for the desired level of link reliability is obtained from the data presented in Figure 6. The factors of T_{on} and R_{on}, represent the time that the transmitter and receiver elements are active, respectively and are derived from packet size and data rate. The front-end components of the design are based on the modulation schemes investigated in this section can be found in Table III. The hardware components are simulated with their respective systems for the purpose of calculating the BER and energy consumption of each modulation scheme.

TABLE III: Front-end components for system design with BPSK, OOK and BFSK modulation

Modulation	Transmitter	Receiver
BPSK	DAC, mix, VCO, PA	ADC, PLL, mix, VCO, filter
OOK	DAC, mix, VCO, PA	ADC, filter
BFSK	DAC, 2 mix, 2 VCO, PA	ADC, 2 filters

The transmitted and received power of a system designed to perform BFSK modulation is calculated as follows:

$$P_{Tx_{BFSK}} = P_{DAC} + 2(P_{mix} + P_{VCO}) + P_{PA} \quad (8)$$

$$P_{Rx_{BFSK}} = P_{ADC} + 2P_{filter} \quad (9)$$

The power of each component is calculated using equations from [20]. These are defined as P_{PA}, P_{mix}, P_{filter}, P_{DAC}, P_{ADC}, P_{PLL} and P_{VCO} and represent the power consumption for the power amplifier (PA), the mixer, the analog filter, the digital to analog converter (DAC), analog to digital converter (ADC), phase locked loop (PLL) and the voltage controlled oscillator (VCO), respectively. We use the operating characteristics of the Teensy MCU, specified in the data sheet, to set parameters of the components utilized in eventual system

design in Section V such as the supply voltage, ADC clock frequency and VCO operating frequency.

Similarly, with the components listed in Table III and equations (8)-(9), the transmitted and received powers for all modulation schemes are calculated. The energy consumption of the entire system for the three candidate modulation schemes is also calculated and represented in Table II using Equation (7).

B. Performance Comparison

Constrained by the physical limitations of the synthetic tissue phantom that is used for empirical validation and the optimal center-frequency gain, we select the channel response generated from the following parameters to compare various systems in the MATLAB environment: a center frequency of 400 kHz, an inter-electrode separation distance of 3 cm, and a total channel length of 10 cm. Figure 6 plots BER versus transmit power (an important limiting factor when considering GC communication within the body). The minimum transmit power needed to obtain the target BER for each modulation scheme is listed in Table II. To fairly compare each technique, the symbol rate is fixed to a value of 50 kbps. Results indicate that the BPSK system offers an improvement in terms of power efficiency and a gradual improvement in terms of bandwidth efficiency, as it is able to achieve the same target BER while occupying less spectrum, and transmitting with less power. However, the performance increase is approximately 3dB when compared to the modulation techniques of OOK and BFSK. At the same time, it can be seen that the energy consumption of BPSK is approximately 18x of the OOK for the GC channel (Table II). These results indicate that the marginal increase in BER performance does not justify the need to increase system complexity, hardware footprint and energy consumption for a low-power wearable. Based on these characteristics, we determine that OOK modulation is better suited at the PHY layer for integration into an embedded system platform for simple biopmetric signal like ECG transmission via GC.

V. Galvanic Coupling System Design

Our prototype system consists of a Teensy microcontroller unit (MCU) with supporting analog front-end hardware for signal modulation and detection. At the fundamental level, the components within the system have the flexibility to implement either of the modulation schemes discussed in Section IV.

A. System Overview

Figure 7a illustrates our design and implementation of a complete system that securely transmits biometric data. The transmitter MCU is configured to transmit with a biometric signature unique to the individual (in our scenario, the ECG signal). To prepare for signal transmission, the pulse width modulation (PWM) output of the Teensy-Tx, combined with controllable internal logic, is toggled based on the binary data and pre-selected bit duration. A low pass filter removes the

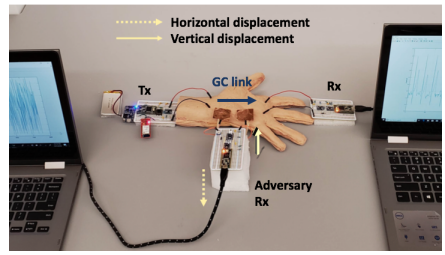

(a)

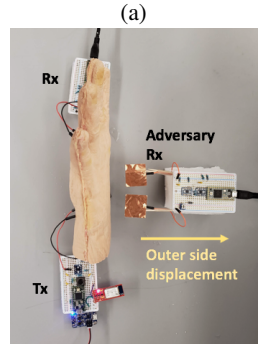

(b)

Fig. 7: Physical GC communication system testbed

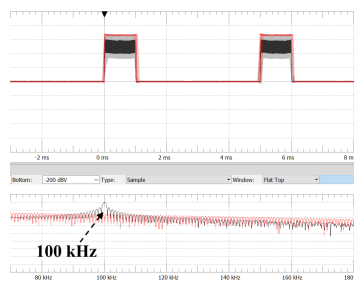

Fig. 8: Transmitted and reproduced signal in time and frequency domain

signal harmonics in the frequency domain, while preserving the center tone ($f_c = 100kHz$). This center frequency is chosen, despite the knowledge of an operating frequency that can yield higher channel gain, due to the gain bandwidth product limitation of the operational amplifier used in receiving chain. The remainder of the parameters utilized in the MATLAB simulation are translated over to the physical domain, and are thus represented in the prototype testbed setup. The data is sent through the tissue wireless channel within the payload of a frame, which consists of a preamble (13-bit Barker code) for synchronization, data length field (8 bits), payload (64 bits) and an 8-bit CRC. Once the signal propagates through the human body channel, the analog front-end receiver hardware utilizes a high pass filter (HPF) to remove any low-frequency noise associated with power-line interference and/or baseline drift. The receiver amplifier (MAX4488 by Maxim Integrated^{TM}) counteracts the attenuation of the channel and high pass filter, while raising the signal level to meet the turn-on voltage requirements of the schottky diode (used in the subsequent system block). Next, we employ an envelope detector circuit to convert the signal back to baseband and to

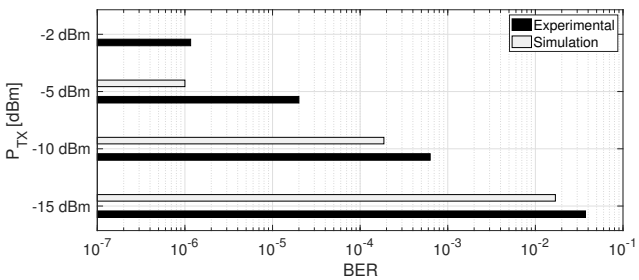

Fig. 9: BER vs transmit power for GC-transceiver OOK modulation

remove any possible carrier wave oscillations that could have an adverse affect on the input to the comparator (MAX4488) trigger at the final stage. The comparator threshold is dynamically controlled through a potentiometer, and it is designed to reproduce the original binary bit sequence delivered from the transmitter. Data packets are detected by the Teensy-Rx, decoded and forwarded through the serial port to MATLAB for subsequent processing.

B. Transceiver Performance

The transmitter and receiver performance is illustrated through the output of an Analog Discovery module. The OOK pulse and its corresponding center tone are generated at the transmitter end. Figure 8 portrays the transmitter and receiver performance in both the time (top) and frequency (bottom) domain. The latter provides validation of the comparator output, returning the original bit sequence that is fed into the ADC of the Teensy-Rx. The former depicts the transmitted signal output. The time domain plots indicate the equivalent bit duration of the two signals, and the frequency domain plots indicate the appropriate operating frequency and that the received signal has been translated from passband to baseband.

We tested the end-to-end link performance by using actual ECG signal traces. Figure 9 depicts the BER for various transmit powers for a link distance of 10 cm. The transmit power is calculated by measuring the impedance of the synthetic tissue phantom across the input terminals of the transmit electrodes, and using the equation $P_{Tx} = V^2/R$. To alter the transmit power levels, we vary the output voltage through the use of a basic attenuator circuit. Observations indicate the experimental capability of achieving a BER of 10^{-6} for a transmit power of -2 dBm (0 BER for simulated trials) and no errors for a transmit power of 0 dBm for both experimental and simulated tests. The power levels that achieved the empirical BER values have been quantified, in [7] and [21], as safe for operation within human tissues, yielding no significant heating effect. Longer distances can be supported, at the expense of higher BER and consequently, higher transmit power, or by introducing forward error correction code.

VI. Over-the-air Signal Susceptibility

To substantiate the claims of a secure biometric transmission system with minimal signal leakage outside the body, we experimentally confirm the level of received signal strength that may be overheard by an over-the-air entity. We evaluate the over-the-air signal susceptibility of our system against the work conducted in [14]-[16], which leverage the use of capacitive coupling (CC) and apply the work in [22] to motivate the use of a hybrid coupling method (GC configuration at the transmitter and CC configuration at the receiver). The purpose of this comparison is to evaluate the susceptibility of our design to over-the-air sniffing against the most commonly used non-RF intra-body communication methods in wearables. We perform a series of experiments where we measure the received signal strength (RSS) and BER of an adversarial receiver with the adequate hardware and software means to attempt signal interception. Thus, the malicious receiver is designed as an exact replica of the receiver presented in Section V only it does not come in physical contact with the phantom. The adversary also consists of two copper electrodes measuring at 3x3 cm with an electrode separation of 5 cm when configured for GC. The RSS and BER are measured at various arrangements representing distances (as shown in Figure 7a and 7b) displaced horizontally (with the palm facing up), vertically and on the outer part of the phantom arm, opposite the side of the tissue where the true receiver is located. Results from Figure 10a illustrate that the RSS at the adversary receiver decreases as we move away from the transmitter in any direction. For all three displacement orientations, the signal strength at the adversary Rx is lowest for the GC method, followed by the hybrid method and then lastly, the CC method. This behavior can be explained from [22] as the hybrid method forms a return path through the environment (as in the CC case) but its range is confined to a portion of the body, that in which the transmitter is located, as opposed to the entire body. Ultimately, these results show the use of GC to transmit a signal in the body provides a more secure channel where the average RSS at the adversary Rx is at the noise floor at a distance of 13 cm, making decoding very difficult. To confirm the level of decoding at the adversary Rx, we conduct the second set of experiments to measure the adversary BER at different positions around the phantom, identical to those in the RSS studies. The results of Figure 10b indicate that the adversarial Rx with GC configuration does not have the capability to decode the signal at any distance or orientation. The CC configuration, however, allows for significantly lower BER values in distances up to 15 centimeters with nearly a 10^{-4} BER at distance of 1 cm away from the tissue, which can lead to a sniffing attack. We thereby conclude that the choice of GC as the method of intra-body communication for our system is advantageous in establishing a secure channel to transmit biometric data.

VII. Discussion and Conclusions

We developed a model of the tissue communication channel by using equivalent electrical circuits that matched closely with experimental testbed measurements. We identified OOK as the preferred modulation technique for our application, and developed a proof-of-concept testbed composed of an embedded system implementation with supporting hardware

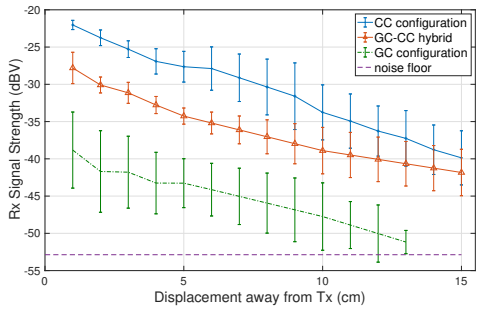

(a)

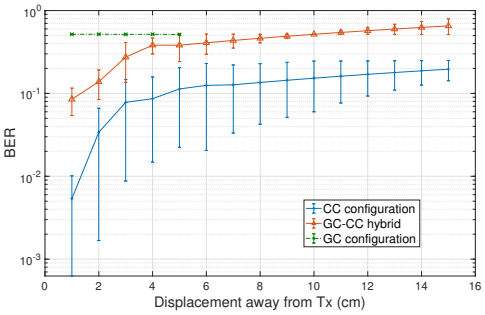

(b)

Fig. 10: Average RSS (a) and BER (b) at adversary Rx at various distances from Tx

and a synthetic tissue phantom. The system functions reliably, transmitting a sample ECG signal over a 10 cm human tissue path with a transmit power of -2 dBm, while maintaining a BER of 10^{-6}. We also demonstrated the GC-secure method of transmitting biometric information by measuring the level of over-the-air signal leakage from the vantage point of an adversarial receiver with satisfactory knowledge of our system design. Our future approach will be focused on exploring the utility of ECG and other biological signals for the development of an end-to-end biometric authentication system and developing ways to transmit the GC-signal over longer distances. Furthermore, we will devise adaptive modulation schemes and reconfigurable front-ends that may adapt the link/physical layer operation based on changing authentication needs or wearable sensor data reporting rates.

Acknowledgment

This material is based on the work supported by the U.S. National Science Foundation under Grant No. CNS-1740907.

References

[1] M. Swaminathan, F. S. Cabrera, J. S. Pujol, U. Muncuk, G. Schirner, and K. R. Chowdhury, "Multi-path model and sensitivity analysis for galvanic coupled intra-body communication through layered tissue," *IEEE Transactions on Biomedical Circuits and Systems*, vol. 10, no. 2, pp. 339–351, April 2016.

[2] A. Pal, A. Kumar Gautam, and Y. Singh, "Evaluation of bioelectric signals for human recognition," vol. 48, pp. 747–753, 12 2015.

[3] A. Fratini, M. Sansone, P. Bifulco, and M. Cesarelli, "Individual identification via electrocardiogram analysis," in *Biomedical engineering online*, 2015.

[4] X. Zhai, A. Amira, and F. Bensaali, "Ecg security identification system on the zynq soc platform," in *2015 IEEE International Conference on Computer and Information Technology; Ubiquitous Computing and Communications; Dependable, Autonomic and Secure Computing; Pervasive Intelligence and Computing*, Oct 2015, pp. 1164–1169.

[5] "Nymi white paper." [Online]. Available: https://nymi.com/

[6] A. Goldberg, L. Amaral, L. Glass, J. M. Hausdorff, P. C. Ivanov, R. Mark, J. E. Mietus, G. B. Moody, C.-K. Peng, E. Stanley, and et al., "Physiobank, physiotoolkit, and physionet: Components of a new research resource for complex physiologic signals," Mar 2018. [Online]. Available: https://www.ahajournals.org/doi/full/10.1161/circ.101.23.e215

[7] W. J. Tomlinson, S. Banou, C. Yu, M. Stojanovic, and K. R. Chowdhury, "Comprehensive survey of galvanic coupling and alternative intra-body communication technologies," *IEEE Communications Surveys Tutorials*, pp. 1–1, 2018.

[8] Z. Cai, M. Seyedi, W. Zhang, F. Rivet, and D. T. H. Lai, "Characterization of impulse radio intrabody communication system for wireless body area networks," *Journal of Medical and Biological Engineering*, vol. 37, no. 1, pp. 74–84, Feb 2017. [Online]. Available: https://doi.org/10.1007/s40846-016-0198-9

[9] M. H. Seyedi, *A Novel Intrabody Communication Transceiver for Biomedical Applications*, 2014. [Online]. Available: http://vuir.vu.edu.au/25847/

[10] H. Baldus, S. Corroy, A. Fazzi, K. Klabunde, and T. Schenk, "Human-centric connectivity enabled by body-coupled communications," *IEEE Communications Magazine*, vol. 47, no. 6, pp. 172–178, June 2009.

[11] T. Kang, K.-I. Oh, H. Park, and S. Kang, "Review of capacitive coupling human body communications based on digital transmission," *ICT Express*, vol. 2, no. 4, pp. 180 – 187, 2016, special Issue on Emerging Technologies for Medical Diagnostics. [Online]. Available: http://www.sciencedirect.com/science/article/pii/S2405959516301710

[12] K. Ito and Y. Hotta, "Signal path loss simulation of human arm for galvanic coupling intra-body communication using circuit and finite element method models," in *2015 IEEE Twelfth International Symposium on Autonomous Decentralized Systems*, March 2015, pp. 230–235.

[13] M. S. Wegmueller, M. Oberle, N. Felber, N. Kuster, and W. Fichtner, "Signal transmission by galvanic coupling through the human body," *IEEE Transactions on Instrumentation and Measurement*, vol. 59, no. 4, pp. 963–969, April 2010.

[14] C. Holz and M. Knaust, "Biometric touch sensing: Seamlessly augmenting each touch with continuous authentication," in *Proceedings of the 28th Annual ACM Symposium on User Interface Software & Technology*, ser. UIST '15. New York, NY, USA: ACM, 2015, pp. 303–312. [Online]. Available: http://doi.acm.org/10.1145/2807442.2807458

[15] M. Hessar, V. Iyer, and S. Gollakota, "Enabling on-body transmissions with commodity devices," in *Proceedings of the 2016 ACM International Joint Conference on Pervasive and Ubiquitous Computing*, ser. UbiComp '16. New York, NY, USA: ACM, 2016, pp. 1100–1111. [Online]. Available: http://doi.acm.org/10.1145/2971648.2971682

[16] J. Yang and A. Sample, "Em-comm: Touch-based communication via modulated electromagnetic emissions," vol. 1, pp. 1–24, 09 2017.

[17] "Dielectric properties of body tissues." [Online]. Available: http://niremf.ifac.cnr.it/tissprop/

[18] B. Infantolino and J. Challis, "Architectural properties of the first dorsal interosseous," vol. 216, pp. 463–9, 04 2010.

[19] F. K. M., K. Sumiko, P.-T. Kia, and P. C. C., "Radial and ulnar cortical thickness of the second metacarpal," *Journal of Bone and Mineral Research*, vol. 10, no. 12, pp. 1930–1934. [Online]. Available: https://onlinelibrary.wiley.com/doi/abs/10.1002/jbmr.5650101212

[20] Y. Li, B. Bakkaloglu, and C. Chakrabarti, "A system level energy model and energy-quality evaluation for integrated transceiver front-ends," *IEEE Transactions on Very Large Scale Integration (VLSI) Systems*, vol. 15, no. 1, pp. 90–103, Jan 2007.

[21] M. Swaminathan, U. Muncuk, and K. R. Chowdhury, "Tissue safety analysis and duty cycle planning for galvanic coupled intra-body communication," in *2016 IEEE International Conference on Communications (ICC)*, May 2016, pp. 1–6.

[22] J. Bae and H. J. Yoo, "The effects of electrode configuration on body channel communication based on analysis of vertical and horizontal electric dipoles," *IEEE Transactions on Microwave Theory and Techniques*, vol. 63, no. 4, pp. 1409–1420, April 2015.